Chinese Chemical Letters 34 (2023) 107359

Contents lists available at ScienceDirect

Chinese Chemical Letters

journal homepage: www.elsevier.com/locate/cclet

General synthesis of Pt and Ni co-doped porous carbon nanofibers to boost HER performance in both acidic and alkaline solutions

Jiaqi Xu, Mengxiao Zhong, Na Song, Ce Wang, Xiaofeng Lu*

Alan G. MacDiarmid Institute, College of Chemistry, Jilin University, Changchun 130012, China

ARTICLE INFO

Article history:
Received 24 November 2021
Revised 24 January 2022
Accepted 20 March 2022
Available online 23 March 2022

Keywords:
Electrospinning
Platinum
Nickel
Porous carbon nanofibers
Hydrogen evolution reaction

ABSTRACT

It is essential to develop efficient electrocatalysts to generate hydrogen from water electrolysis for hydrogen economy. In this work, platinum (Pt) and nickel (Ni) co-doped porous carbon nanofibers (Pt/Ni-PCNFs) with low Pt content were prepared *via* an electrospinning, carbonization and galvanic replacement reaction. Because of the high electrical conductivity, abundant electrochemical active sites and synergistic effect between Pt and Ni nanoparticles, the optimized Pt/Ni-PCNFs catalyst shows an excellent HER activity with overpotentials of 20 mV in 0.5 mol/L H_2SO_4 and 46 mV in 1 mol/L KOH at a current density of 10 mA/cm^2. Furthermore, over 35-h long-term stability has been achieved without significant attenuation. This work provides a simple route to prepare highly efficient electrocatalysts for water splitting and has great prospects in the field of renewable energy.

In recent years, due to the limited reserves of fossil fuels and their causing certain pollutions to the environment, the energy problem needs to be solved urgently [1,2]. Clean hydrogen energy has attracted more and more attention from the society. The electrochemical water splitting reaction is regarded as one of the most important means for the sustainable production of hydrogen [3,4]. The platinum (Pt)-based catalyst is proven to be the most efficient hydrogen evolution reaction (HER) electrocatalyst so far [5]. However, due to the high cost and scarcity of platinum on the earth, reducing the amount of Pt in the catalyst while ensuring high catalytic performance has become a top priority [6]. The integration of Pt with other low-cost transition metals can effectively reduce the use of precious metals, and at the same time, due to the synergistic effect of the two metals, the HER performance of the material can be enhanced significantly [7–9]. For example, Ojani and co-workers reported a facile galvanic replacement strategy to prepare bimetallic Pd/Pt microstructures toward HER, showing a much better electrocatalytic activity than pure Pt in the acidic electrolyte [10]. Another example presented the fabrication of Ir/Pt electrodes *via* a spontaneous deposition route as efficient HER catalyst in an alkaline solution, which showed a superior catalytic activity compared with the bare Pt and Ir electrodes [11].

Although Pt-based catalysts display excellent HER performance in either acidic and alkaline media, a significant challenge of them toward HER is their unsatisfied stability in alkaline condition, which might be related to their poor resistance to alkali corrosion. Therefore, it is a good idea to incorporate Pt clusters or nanoparticles into a conducting matrix to improve the durability of the catalyst. In addition, the conducting matrix can prevent the aggregation of the Pt nanoparticles and a synergistic effect may be generated between the active Pt component and the matrix. Among several typical conducting matrices, carbon nanofibers (CNFs) are considered as a type of superior catalyst matrix due to their large specific surface area, high electrical conductivity and excellent stability [12–14]. Electrospinning technology is a simple and controllable way to produce CNFs [15,16]. Furthermore, through the manipulation of the composition of the spinning solution and subsequent carbonization process, the encapsulation of metal and other ceramic components into the CNFs can be easily achieved, which is beneficial to promote the electrocatalytic performance [17–19]. For example, a direct electrospinning-carbonization route has been developed to prepare both Co and Mo_2C nanoparticles embedded in nitrogen-doped CNFs coupled with carbon nanotubes (Co/Mo_2C-NCNTs) as both efficient HER and oxygen evolution reaction (OER) electrocatalysts in an alkaline medium, however, such strategy could not ensure the formation of unique interface between Co and Mo_2C components, which significantly affect their greatly enhanced electrocatalytic activity [20].

Herein, we report the preparation of Pt and nickel (Ni) co-doped porous carbon nanofibers (Pt/Ni-PCNFs) as highly efficient HER electrocatalyst through an electrospinning-carbonization-galvanic replacement process. The replacement reaction between Ni nanoparticles and H_2PtCl_6 enables the formation of Ni and Pt

* Corresponding author.
E-mail address: xflu@jlu.edu.cn (X. Lu).

https://doi.org/10.1016/j.cclet.2022.03.082
1001-8417/

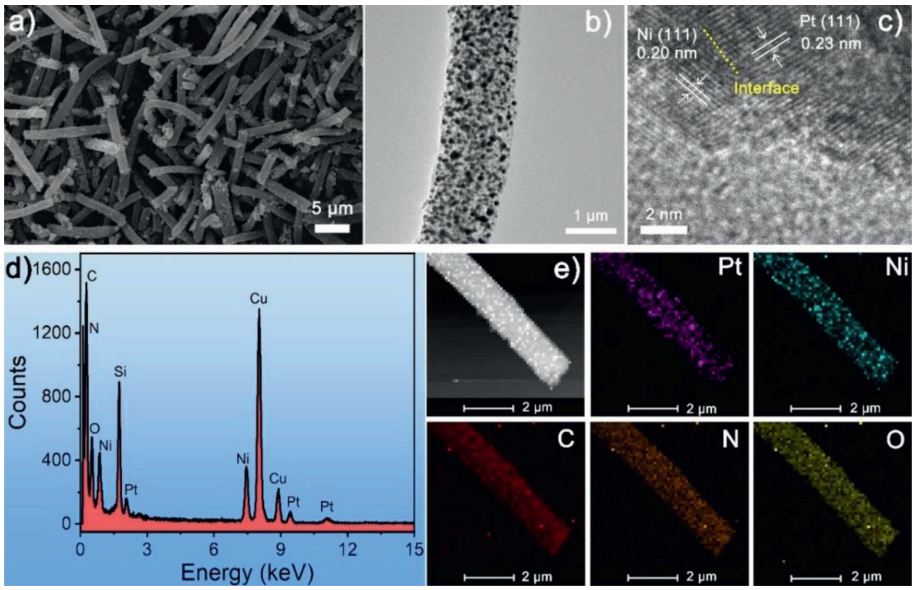

Fig. 1. (a) SEM image of Pt/Ni-PCNFs-50. (b) TEM image of a single Pt/Ni-PCNFs-50 nanofiber. (c) HRTEM image of a single Pt/Ni-PCNFs-50 nanofiber. (d) EDX spectrum of Pt/Ni-PCNFs-50 nanofibers. (e) HAADF-STEM image and EDX element mappings of Pt, Ni, C, N and O elements in Pt/Ni-PCNFs-50 nanofibers.

nanoparticles with a unique interface, which is beneficial for the superior HER performance. Then the optimized Pt/Ni-PCNFs sample with a low Pt amount shows an excellent HER performance with a mass activity (MA) of 3.94 and 2.48 times as high as that of benchmark Pt/C catalyst in acidic and alkaline conditions, respectively. This work provides a new strategy for the construction of highly efficient HER catalysts.

The overall synthetic route of Pt/Ni-PCNFs mainly involves four steps. First, an electrospinning way is performed to fabricate metal organic framework-zeolitic imidazolate framework-8 (ZIF-8)/polyacrylonitrile (PAN)-polyvinylpyrrolidone (PVP) nanofibers. Scanning electron microscopy (SEM) images (Figs. S1a and b in Supporting information) display the uniform fiber-like morphology with a smooth surface, illustrating the complete encapsulation of ZIF-8 particles in the fibers. When the PVP is removed, it can also be clearly seen that porous PAN (PPAN) fibers are obtained resulting from the empty space and dense ZIF-8 particles are evenly distributed throughout the PPAN fibers (Figs. S1c and d in Supporting information). Second, after a further treatment with the nickel salt, Ni precursor/PPAN fibers have been achieved, presenting a similar morphology with that of ZIF-8/PPAN product (Fig. S2 in Supporting information). Third, the Ni precursor/PPAN fibers are carbonized under an inert atmosphere to produce Ni/PCNFs. As shown in Fig. S3a and b (Supporting information), the prepared Ni/PCNFs reserve the fiber-like morphology while their surface becomes rough, and a lot of Ni nanoparticles with sizes of tens of nanometers are encapsulated in the PCNFs. Furthermore, TEM image can also reveal the porous structure of the Ni/PCNFs. Finally, through a galvanic replacement, Pt/Ni-PCNFs with a distinct interface between Pt and Ni nanoparticles are obtained, which still shows a fiber-like morphology with a diameter ranging from 1.1 μm to 1.5 μm (Fig. 1a). Similar with those of Ni/PCNFs, Pt and Ni nanoparticles are well distributed within entire the PCNFs (Fig. 1b). The HRTEM image (Fig. 1c) shows the crystal plane spacing of 0.20 and 0.23 nm, corresponding to the (111) crystal plane of Ni and the (101) crystal plane of Pt, respectively. More specifically, a distinct interface between Pt and Ni nanoparticles is observed, which is beneficial for their electrocatalytic property. In addition, energy dispersive X-ray (EDX) spectrum exhibits Pt, Ni, C, N and O signals in Pt/Ni-PCNFs sample (Fig. 1d). Among them, the signal of Pt is relatively weak, demonstrating the low content of Pt in the sample. The exact percentage of Pt in Pt/Ni-PCNFs-50 is further determined by inductively coupled plasma (ICP) measurements, showing a weight percentage of 4.3 wt% (Table S1), which is in accordance with the EDX result. It is worth noting that Si and Cu signals, which appear in the EDX spectrum, stem from the instrument and TEM sample support. The high angle annular dark-field scanning TEM (HAADF-STEM) (Fig. 1e) and EDX element mapping also clearly reveal the uniform distribution of Pt, Ni, C, N and O elements, indicating that Pt and Ni are uniformly integrated in the entire PCNFs. Furthermore, we have also investigated the influence of the Pt precursor content on the formation of Pt and Ni nanoparticles in the Pt/Ni-PCNFs. It is found that the morphology of the fiber and the size of Pt and Ni nanoparticles do not change significantly, while the density of the metal nanoparticles increase a little with the increasing of the Pt precursor content (Figs. S3c–f in Supporting information).

X-ray diffraction (XRD) patterns reveal the structural information of the crystalline properties of the prepared samples, which are shown in Fig. 2a. The peaks near at 44.5°, 51.8° and 76.4° in the XRD pattern of Ni-PCNFs can be attributed to the (111), (200) and (220) crystal planes of Ni (JCPDS No. 04-0850), respectively. With the introduction of Pt, the characteristic peaks of Pt element appear in Pt/Ni-PCNFs-50 and Pt/Ni-PCNFs-100. In Pt/Ni-PCNFs-50, the peak at 39.9° corresponds to the (111) crystal plane of Pt (JCPDS No. 04-0802). In addition, in Pt/Ni-PCNFs-100, three other diffraction peaks at 46.4°, 67.5°, and 81.4° corresponding to the (200), (220) and (311) crystal planes of Pt are also observed, demonstrating that Ni nanoparticles are partially replaced by Pt component to form Pt/Ni composite.

X-ray photoelectron spectroscopy (XPS) has been further used to study the composition and valence of elements in the prepared catalysts. The full survey spectrum of Pt/Ni-PCNFs-50 shows the presence of Pt, Ni, C, N and O elements (Fig. S4 in Supporting information). Fig. 2b exhibits two peaks of Pt 4f at 72.1 and 75.3 eV, corresponding to the Pt $4f_{7/2}$ and Pt $4f_{5/2}$ tracks, respectively [21,22], which indicates the successful introduction of Pt. As shown in Fig. 2c, the XPS fine spectra of Ni 2p can be divided into four peaks, and the Ni $2p_{3/2}$ and Ni $2p_{1/2}$ peaks are presented at 855.7 and 873.5 eV, respectively, indicating the formation of metallic Ni in Pt/Ni-PCNFs-50. In addition, two satellite peaks appearing at the positions of 861.3 and 879.6 eV demonstrate the partial oxidation of Ni to NiO [23,24], which is beneficial to enhance the water

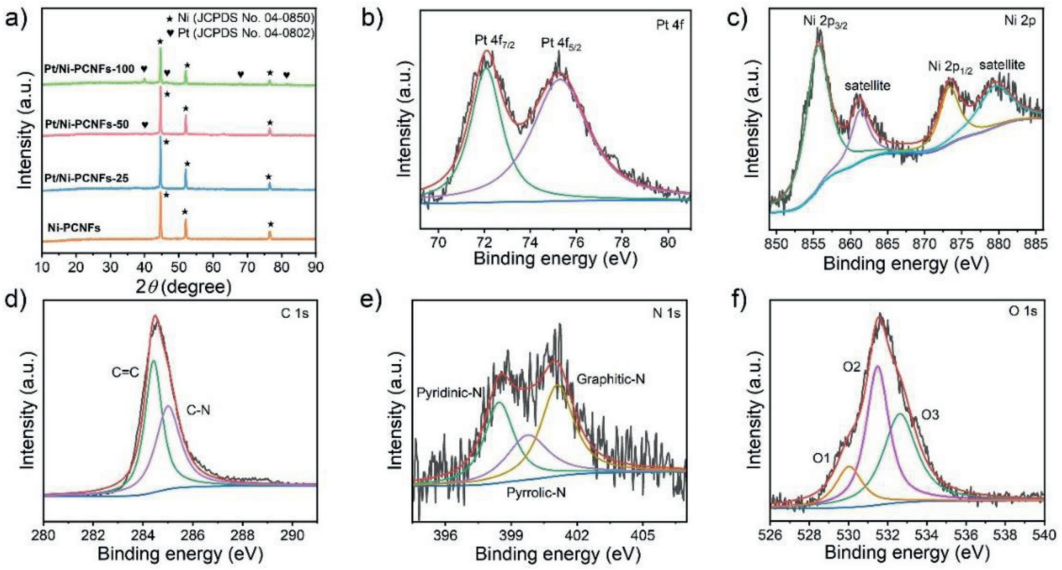

Fig. 2. (a) XRD patterns of Pt/Ni-PCNFs-25, Pt/Ni-PCNFs-50, Pt/Ni-PCNFs-100 and Ni-PCNFs. XPS spectra of Pt/Ni-PCNFs-50: (b) Pt 4f, (c) Ni 2p, (d) C 1s, (e) N 1s and (f) O 1s.

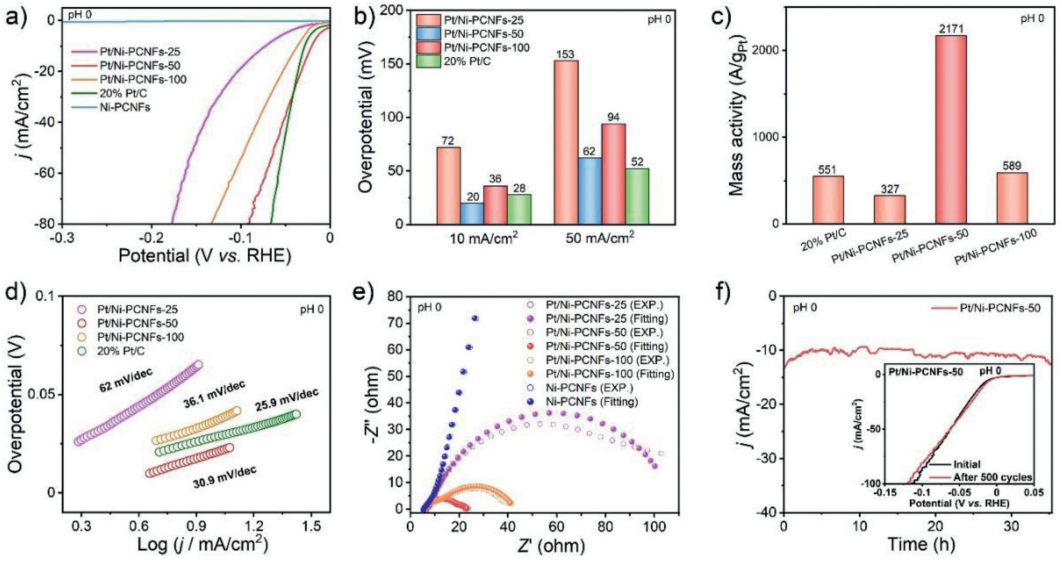

Fig. 3. HER measurement in 0.5 mol/L H_2SO_4. (a) LSV curves of different catalysts. (b) The overpotentials of different catalysts at 10 and 50 mA/cm^2. (c) The MA at the overpotential of 50 mV. (d) Tafel plots derived from corresponding LSV curves. (e) Nyquist plots perform for each sample. (f) The *i-t* responses of Pt/Ni-PCNFs-50 nanofibers at an overpotential of 33 mV, the inset shows the LSV curves before and after 500 CV cycles.

dissociation. In Fig. 2d, two peaks of C 1s at 284.4 and 285.0 eV positions correspond to C=C and C–N, respectively [19]. In addition, three peaks at 398.4, 399.8 and 401.1 eV shown from the high resolution XPS spectrum of N 1s correspond to pyridine N, pyrrole N and graphite N, respectively (Fig. 2e) [25]. Fig. 2f shows the O 1s spectrum of Pt/Ni-PCNFs-50, where the O1 peak at 530.0 eV can be interpreted as a metal-oxygen bond. The O2 peak at 531.5 eV has the characteristics of oxygen in hydroxide, indicating the presence of a certain number of nickel hydroxide on the surface of the catalyst, which is beneficial to improve the adsorption of water, thereby increasing the activity of HER. The O3 component with a peak position of 532.6 eV may be related to the physicochemical adsorption of water molecules by the catalyst [26].

The electrochemical HER measurements of Pt/Ni-PCNFs were firstly performed in an acidic electrolyte to evaluate the electrocatalytic performance, with commercial Pt/C and Ni-PCNFs as references. Fig. 3a shows the linear sweep voltammetry (LSV) curves of several catalysts under acidic conditions after iR compensation, demonstrating that Pt/Ni-PCNFs-50 exhibits even a better electrocatalytic activity than commercial Pt/C catalyst. Typically, as shown in Fig. 3b, the overpotentials of several catalysts at current densities of 10 and 50 mA/cm^2 are compared. Among them, the overpotentials of Pt/Ni-PCNFs-50 are 20 and 62 mV, respectively, which are lower than that of Pt/Ni-PCNFs-100 (36 and 94 mV), Pt/Ni-PCNFs-25 (72 and 153 mV) and comparable with the Pt/C catalyst (28 and 52 mV), while Ni-PCNFs almost have no HER activity under the measurement condition. For comparison, we have also prepared Pt/Ni-CNFs-50 catalyst that is synthesized without the addition of PVP, showing a higher overpotential of 81 mV compared with the Pt/Ni-PCNFs-50, which demonstrates that the porous structure benefits to promote the HER performance (Fig. S5 in Supporting information). In addition, MA is also used to estimate the HER performance of the catalysts. The MA value of Pt/Ni-PCNFs-50 is the highest among the prepared catalysts, which is

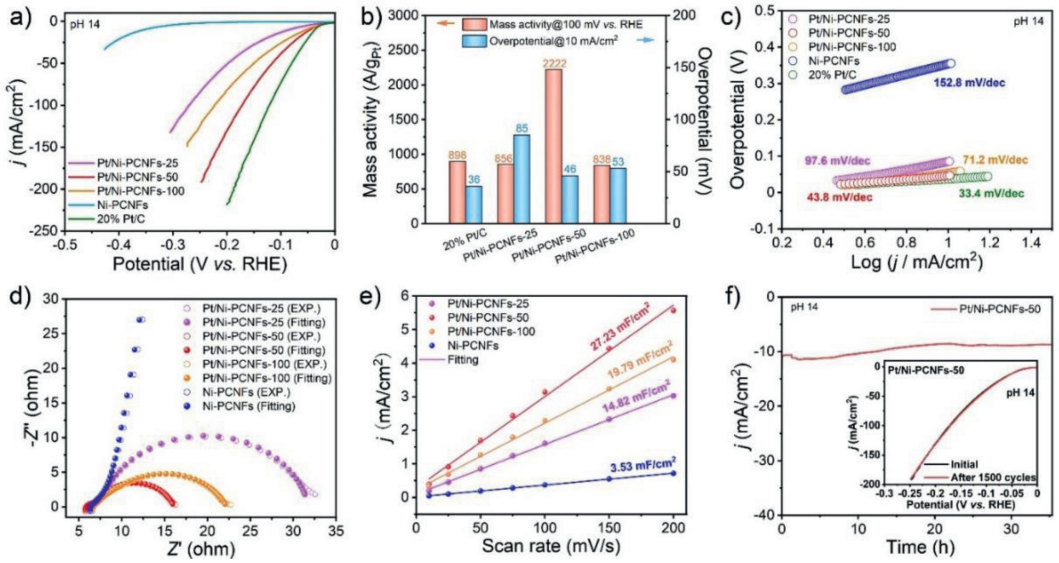

Fig. 4. The HER measurement in 1 mol/L KOH. (a) LSV curves of different catalysts. (b) The MA at the overpotential of 100 mV and the overpotentials at 10 mA/cm^2 of different catalysts. (c) Tafel plots derived from corresponding LSV curves. (d) Nyquist plots for each sample. (e) The capacitive current density of as-prepared samples at different scan rates. (f) The *i-t* responses of Pt/Ni-PCNFs-50 catalyst at an overpotential of 44 mV, the inset shows the LSV curves before and after 1500 CV cycles.

3.94 times as high as that of commercial Pt/C, confirming its excellent intrinsic electrocatalytic activity toward HER (Fig. 3c).

To further study the reaction kinetics of the catalysts in 0.5 mol/L H_2SO_4, the Tafel slope diagram is provided in Fig. 3d. The Tafel slope of Pt/Ni-PCNFs-50 (30.9 mV/dec) is smaller than that of Pt/Ni-PCNFs-100 (36.1 mV/dec) and Pt/Ni-PCNFs-25 (62 mV/dec), demonstrating its fast reaction kinetics during HER process. In addition, the electrochemical impedance of the catalysts has also been tested. The equivalent circuit diagram of the impedance curve fitting process is shown in Fig. S6 (Supporting information). As shown in Fig. 3e, Pt/Ni-PCNFs-50 sample shows the smallest semicircle, and the fitted charge transfer resistance (R_{ct}) is calculated to be 16.6 Ω, which is smaller than other control catalysts, indicating the high conductivity and fast electron transfer rate of Pt/Ni-PCNFs-50 catalyst.

Durability is also an important parameter to evaluate the performance of electrocatalysts. The chronoamperometric measurement is carried out by loading the catalyst on a carbon paper (Fig. 3f). After over 35 h of continuous testing, the current-time (*i-t*) curve of Pt/Ni-PCNFs-50 catalyst shows a good stability, and there was no significant drop in the overall current trend. The slight fluctuation of the curve may be due to the accumulation and release of bubbles on the electrode surface. In addition, continuous CV cycles are conducted on the RDE to show that the LSV curve of the Pt/Ni-PCNFs-50 recorded after 500 cycles shows a little decreasing overpotential to reach 10 mA/cm^2 compared to the initial curve (Fig. 3f, inset), demonstrating the moderate long-term stability of the Pt/Ni-PCNFs-50 catalyst in an acidic medium.

In addition to the acidic medium, Pt/Ni-PCNFs-50 also exhibits an excellent HER performance in an alkaline solution. Fig. 4a shows the LSV curves of different catalysts in 1.0 mol/L KOH after iR compensation. It is found that the prepared Pt/Ni-PCNFs-50 shows a low overpotential of 46 mV when the current density $j = 10$ mA/cm^2, which is lower than Pt/Ni-PCNFs-100 (53 mV), Pt/Ni-PCNFs-25 (85 mV), Ni-PCNFs (353 mV), and the Pt/Ni-CNFs-50 catalyst that is synthesized without the addition of PVP (86 mV) (Fig. S5 in Supporting information). This overpotential is a little higher than that of commercial Pt/C catalyst (36 mV), however, the MA value of Pt/Ni-PCNFs-50 is the highest among all the control catalysts, which is even 2.47 times as high as that of 20% Pt/C, presenting its excellent intrinsic electrocatalytic activity toward HER in an alkaline condition (Fig. 4b). The Tafel plots have also been obtained from the LSV curves (Fig. 4c), demonstrating a lower value of Pt/Ni-PCNFs-50 (43.8 mV/dec) than Pt/Ni-PCNFs-100 (71.2 mV/dec), Pt/Ni-PCNFs-25 (97.6 mV/dec), and Ni-PCNFs (152.8 mV/dec), illustrating the fast inherent HER reaction kinetics and charge transfer rate in alkaline solution.

We have also tested the electrochemical impedance of the catalysts in 1 mol/L KOH electrolyte. From Fig. 4d, it can be found that the prepared Pt/Ni-PCNFs-50 has R_{ct} of 9.04 Ω, which is closely related to its good electron transport ability and efficient reaction kinetics. To estimate the electrochemically active surface area (ECSA) of Pt/Ni-PCNFs, the electrochemical double-layer capacitance (C_{dl}) is calculated by cyclic voltammetry (CV) measurements. From Fig. S7 (Supporting information), the C_{dl} value of Pt/Ni-PCNFs-50 is calculated to be 27.23 mF/cm^2, which is higher than that of Pt/Ni-PCNFs-100 (19.79 mF/cm^2), Pt/Ni-PCNFs-25 (14.82 mF/cm^2), and Ni-PCNFs (3.53 mF/cm^2) (Fig. 4e). As the ECSA is proportional to the C_{dl}, the largest C_{dl} value indicates that Pt/Ni-PCNFs-50 possesses the largest exposed active sites resulting from the porosity of the material and the unique interface between Ni and Pt NPs, which is beneficial for the superior HER performance. Finally, we tested the long-term stability of Pt/Ni-PCNFs-50 under an alkaline condition. As shown in Fig. 4f, after over 35 h of continuous testing, the current density of the catalyst does not change much, demonstrating the excellent durability. Moreover, the current density hardly decreased after 1500 CV cycles, which also illustrates the favorable stability of the catalyst (Fig. 4f, inset).

Furthermore, the Pt/Ni-PCNFs-50 catalyst is thoroughly characterized after HER process to understand the mechanism of the favorable stability. Firstly, the morphology and chemical structure of the Pt/Ni-PCNFs-50 catalyst after the HER stability test in an alkaline medium have been studied. As shown in the SEM image (Fig. S8a in Supporting information), the fiber structure of Pt/Ni-PCNFs-50 is well maintained. XRD and XPS measurements have also been used to characterize the chemical structure of the Pt/Ni-PCNFs-50 catalyst after the HER measurement in 1 mol/L KOH electrolyte, both showing the similar typical peaks with the initial Pt/Ni-PCNFs-50 catalyst (Figs. S8b–d in Supporting information). Similarly, the SEM image and XRD pattern of the Pt/Ni-PCNFs-50 catalyst after the stability test in an acidic medium have also presented the identical morphologies and chemical structures with

the initial electrocatalyst (Fig. S9 in Supporting information). These results suggest that the Pt/Ni-PCNFs catalyst is highly stable during the long-term HER process.

The superior HER performance of Pt/Ni-PCNFs-50 in both acidic and alkaline media can be ascribed to the following factors: (1) PCNFs are excellent conducting substrate with a favorable chemical stability, which can inhibit the corrosion of Pt and Ni nanoparticles. Furthermore, the porous structure is conducive to the entry of electrolyte and the release of generated gas during the HER process. (2) The encapsulation of Pt and Ni nanoparticles derived from the framework of ZIF-8 provides more exposed electrochemical active sites, resulting in fast dynamics and excellent HER activity. (3) The distinct interface between Pt and Ni nanoparticles can regulate their electronic structure to improve the adsorption of the reaction intermediates and the desorption of the hydrogen product, exhibiting a synergistic catalytic effect toward HER.

In summary, we have demonstrated a simple and efficient strategy to prepare a new HER electrocatalyst with an excellent electrocatalytic performance in both acidic and alkaline media. The HER performance is greatly influenced by the Pt content in the Pt/Ni-PCNFs. Due to the advantages of the conducting and porous structure of PCNFs as well as the synergistic effect between Pt and Ni nanoparticles, the prepared Pt/Ni-PCNFs show a superior HER activity with low overpotential and large MA as well as excellent long-term stability. All in all, this work offers a novel route to fabricate high-efficiency HER electrocatalysts and broadens their applications in the field of energy conversion and storage.

Declaration of competing interest

The authors declare that they have no conflict of interest.

Acknowledgments

This work was financially supported by the National Natural Science Foundation of China (Nos. 5197307, 219875084) and the Project of the Education Department of Jilin Province, China (No. JJKH20211047KJ).

Supplementary materials

Supplementary material associated with this article can be found, in the online version, at doi:10.1016/j.cclet.2022.03.082.

References

[1] X.X. Zhang, G.M. Qu, Z.H. Wang, et al., Chin. Chem. Lett. 32 (2021) 2453–2458.
[2] G.T. Xiang, Y. Meng, G.M. Qu, et al., Sci. Bull. 65 (2020) 443–451.
[3] M. Caban-Acevedo, M.L. Stone, J.R. Schmidt, et al., Nat. Mater. 14 (2015) 1245–1251.
[4] E.S. Liu, J.K. Li, L. Jiao, et al., J. Am. Chem. Soc. 141 (2019) 3232–3239.
[5] S.L. Zhang, X.F. Lu, Z.P. Wu, D.Y. Luan, X.W. Lou, Angew. Chem. Int. Ed. 60 (2021) 1–7.
[6] S. Bai, C.M. Wang, M.S. Deng, et al., Angew. Chem. Int. Ed. 53 (2014) 12120–12124.
[7] C. Cui, R.F. Cheng, C. Zhang, X.H. Wang, Chin. Chem. Lett. 31 (2020) 988–991.
[8] H.Y. Jin, X. Liu, S.M. Chen, et al., ACS Energy Lett. 4 (2019) 805–810.
[9] P.T. Wang, K.Z. Jiang, G.M. Wang, J.L. Yao, X.Q. Huang, Angew. Chem. Int. Ed. 55 (2016) 12859–12863.
[10] R. Ojani, J.B. Raoof, E. Hasheminejad, Int. J. Hydrog. Energy 38 (2013) 92–99.
[11] S. Štrbac, M. Smiljanić, T. Wakelin, J. Potočnik, Z. Rakočevićb, Electrochim. Acta 306 (2019) 18–27.
[12] L. Han, S.J. Dong, E.K. Wang, Adv. Mater. 28 (2016) 9266.
[13] X.F. Lu, C. Wang, F. Favier, N. Pinna, Adv. Energy Mater. 7 (2017) 1601301.
[14] W. Li, C. Wang, X. Lu, J. Mater. Chem. A 9 (2021) 3786–3827.
[15] J. Xue, T. Wu, Y. Dai, Y. Xia, Chem. Rev. 119 (2019) 5298–5415.
[16] W. Song, M.X. Li, C. Wang, X.F. Lu, Carbon Energy 3 (2021) 101–128.
[17] M.X. Li, Y. Zhu, H.Y. Wang, et al., Adv. Energy Mater. 9 (2019) 1803185.
[18] T. Li, S. Li, Q. Liu, et al., Adv. Sci. 7 (2020) 1902371.
[19] J. Zhang, W. Jia, S. Dang, Y. Cao, J. Colloid Interface Sci. 560 (2020) 161–168.
[20] J. Zhang, X.P.P. Sun, P. Wei, et al., ChemCatChem 12 (2020) 3737–3745.
[21] X.X. Pan, S.L. Lu, D. Zhang, et al., J. Mater. Chem. A 8 (2020) 4911–4919.
[22] K. Wang, Q.L. Yao, S.J. Qing, Z.H. Lu, J. Mater. Chem. A 7 (2019) 9903–9911.
[23] M.X. Li, H.Y. Wang, W.D. Zhu, et al., Adv. Sci. 7 (2020) 1901833.
[24] Q.L. Yao, Z.H. Lu, R. Zhang, et al., J. Mater. Chem. A 6 (2018) 4386–4393.
[25] S.B. Yang, X.L. Feng, X.C. Wang, K. Müllen, Angew. Chem. Int. Ed. 50 (2011) 5339.
[26] Y. Fu, H.Y. Yu, C. Jiang, et al., Adv. Funct. Mater. 28 (2018) 1705094.